Comparison of different methods for analyzing μSR line shapes in the vortex state of type-II superconductors

2009 J. Phys.: Condens. Matter 21 075701

(http://iopscience.iop.org/0953-8984/21/7/075701)

J. Phys.: Condens. Matter **21** (2009) 075701 (15pp) doi:10.1088/0953-8984/21/7/075701

Comparison of different methods for analyzing μSR line shapes in the vortex state of type-II superconductors

A Maisuradze[1,2], R Khasanov[1,2], A Shengelaya[1,3] and H Keller[1]

[1] Physik-Institut der Universität Zürich, Winterthurerstrasse 190, CH-8057 Zürich, Switzerland
[2] Laboratory for Muon Spin Spectroscopy, Paul Scherrer Institut, CH-5232 Villigen PSI, Switzerland
[3] Physics Institute of Tbilisi State University, Chavchavadze 3, GE-0128 Tbilisi, Georgia

E-mail: alexander.maisuradze@psi.ch

Received 29 August 2008, in final form 21 December 2008
Published 19 January 2009
Online at stacks.iop.org/JPhysCM/21/075701

Abstract

A detailed analysis of muon-spin rotation (μSR) spectra in the vortex state of type-II superconductors using different theoretical models is presented. Analytical approximations of the London and Ginzburg–Landau (GL) models, as well as an exact solution of the GL model were used. The limits of the validity of these models and the reliability for extracting parameters such as the magnetic penetration depth λ and the coherence length ξ from the experimental μSR spectra were investigated. The analysis of the simulated μSR spectra showed that at high magnetic fields there is a strong correlation between λ and ξ obtained for any value of the Ginzburg–Landau parameter $\kappa = \lambda/\xi$. The smaller the applied magnetic field, the smaller the possibility of finding the correct value of ξ. A simultaneous determination of λ and ξ without any restrictions is very problematic, regardless of the model used to describe the vortex state. It was found that for extreme type-II superconductors and low magnetic fields, the fitted value of λ is practically independent of ξ. The second-moment method frequently used to analyze μSR spectra by means of a multi-component Gaussian fit generally yields reliable values of λ over the whole range of applied fields $H_{c1} \ll H \lesssim H_{c2}$ (H_{c1} and H_{c2} are the first and second critical fields, respectively). These results are also relevant for the interpretation of small-angle neutron scattering experiments on the vortex state in type-II superconductors.

(Some figures in this article are in colour only in the electronic version)

1. Introduction

The muon-spin rotation (μSR) technique is one of the most powerful and unique tools for studying the internal magnetic field distribution $P(B)$ associated with the vortex lattice in type-II superconductors (see e.g. [1–3]). In the vortex state for an applied magnetic field $H > H_{c1}$, or $B > 0$ (H_{c1} and B are the first critical field and the magnetic induction in a sample, respectively) [4] the energy of the surface separating normal and superconducting fractions of the sample becomes negative and the field penetrates the sample in the form of quantized flux lines, called vortices, each of them containing an elementary flux quantum ($\Phi_0 = h/2e \simeq 2.0678 \times 10^{-15}$ Wb) [5]. In the case of small pinning these vortices arrange themselves in a regular vortex lattice called a flux-line lattice (FLL) [5]. The distribution of the internal magnetic fields $P(B)$ inside the superconducting sample in the vortex state is uniquely determined by two characteristic lengths, the magnetic field penetration depth λ and the coherence length ξ. From μSR experiments, $P(B)$ profiles are obtained by performing a Fourier transformation of the μSR time spectra. There are different approaches for analyzing μSR data. Generally, the magnetic field penetration depth λ is determined from the second moment $\langle \Delta B^2 \rangle$ of the internal field distribution $P(B)$ [6–12]. For an isotropic extreme type-II superconductor ($\lambda \gg \xi$) it was shown that $\langle \Delta B^2 \rangle \propto \lambda^{-4}$ [13]. The more

advanced approaches that allow one to obtain not only λ, but also the coherence length ξ require a theoretical model for the spatial variation of the internal magnetic field $B(\mathbf{r})$ ($\mathbf{r}$ is spatial coordinate). An essential requirement of the model is that it must account for the finite size of the vortex cores. So far, the internal magnetic field distribution $P(B)$ measured using μSR has been analyzed assuming analytical models for $B(\mathbf{r})$ based on London and Ginzburg–Landau (GL) theories. The London theory provides the simplest approach for modeling the FLL. Since London theory does not account for the finite size of the vortex cores, a cut-off factor derived from GL theory must be inserted into the analytical London expression for $B(\mathbf{r})$ to correct for the divergence of $B(\mathbf{r})$ in the vortex core [14, 3]. The GL theory has the spatial dependence of the order parameter built in and thus provides a phenomenological description of the magnetic field profile in the vortex core region. Abrikosov [5] predicted the vortex core state from a periodic solution of the GL equations near the second critical field $B_{c2} = \mu_0 H_{c2}$ and provided an approximate analytical solution of these equations for an isolated vortex for fields of the order of H_{c1}. Clem [15] proposed a variational method for solving the GL equations that was further extended by Hao *et al* [16]. A simplified version of this model for $\lambda/\xi \gg 1$ was developed by Yaouanc *et al* [14], and is often used in the literature [3].

The London and the GL models were widely applied to determine values of λ and ξ from measured μSR time spectra taken in the mixed state of type-II superconductors [17, 14, 18, 3, 19–31]. We should emphasize, however, that despite the broad usage, the limits of validity of these models and the reliability of the parameters extracted from the fits are not much discussed in the literature. The main purpose of the present paper is to address these basic questions. The paper is divided into two parts. In the first part we briefly describe the models often used for the analysis of μSR spectra: the London model with Gaussian cut-off (LG model), the modified London model (ML model), and the analytical Ginzburg–Landau model (AGL model). These models are compared with the most precise model based on the iterative method for solving the Ginzburg–Landau equations developed recently by Brandt [4], the so called numerical Ginzburg–Landau model (NGL model). $P(B)$ profiles for various sets of λ, ξ, and magnetic field B were first simulated by means of the NGL model and then analyzed within the framework of the LG, ML, and AGL models. For further discussions, it is convenient to define the reduced magnetic field $b = B/B_{c2}$. It was found that the ML model can be used *only* for low magnetic fields ($b \lesssim 0.1$), while both the AGL model and the LG model yield reliable results over almost the *whole* magnetic field range. However, the values of λ and ξ obtained by means of the AGL and the LG model deviate systematically from the initial parameters used for the simulated $P(B)$ profiles for magnetic fields in the range $0.01 \lesssim b \leqslant 1$. It was also shown that for $b \lesssim 0.01$ the $P(B)$ profiles do not depend on the coherence length ξ. In the second part of the paper we present a systematic analysis of simulated μSR time spectra (with typical statistics used in real μSR experiments) by means of the LG model. Over the whole field range ($0 < b \leqslant 1$) and for any values of the Ginzburg–Landau parameter $\kappa = \lambda/\xi$ there is a strong correlation between the values of λ and ξ determined from the fit. This implies that an analysis of μSR data using this approach, without taking into account these correlations, may lead to substantial errors in the determination of the absolute values of λ and ξ, and even may result in unphysical dependences of λ and ξ on magnetic field and temperature. In addition, the second-moment method applied to a multiple-Gaussian fit was tested in order to check how reliably the penetration depth λ can be determined by this method. In particular, the influence of the number of Gaussians used in the multi-Gaussian fit on the quality of the fit was investigated. For typical statistics used in the experiment and practically over the whole field range ($0 < b \lesssim 1$), the second-moment method applied to a multi-Gaussian fit may provide correct values for λ within a few per cent.

The paper is organized as follows. In section 2 various theoretical models used to analyze μSR data are briefly described. The dependence of the magnetic field distribution $P(B)$ on λ, ξ, b, and the Gaussian smearing parameter σ_g, as calculated within the LG model, is discussed in section 3. In section 4 we compare the results obtained by means of the models described in section 2 for the case of an extreme type-II superconductor ($\kappa = \lambda/\xi \gg 1$). Section 5 comprises the studies of the simulated μSR data. The simulated μSR spectra were analyzed by means of the various models described in section 2 in order to search for possible correlations between the parameters, such as λ, ξ, and σ_g. The conclusions follow in section 6.

2. Models for data analysis

As mentioned in section 1, the simplest and the most widely used approach for analyzing μSR data is based on the relation between the magnetic penetration depth λ and the second moment $\langle \Delta B^2 \rangle$ of the internal field distribution $P_{id}(B)$ of the ideal FLL [13, 4, 32]:

$$\lambda^{-4} = C \langle \Delta B^2 \rangle. \tag{1}$$

Here, C is the proportionality coefficient depending on the value of the reduced magnetic field $b = \langle B \rangle / B_{c2}$ ($\langle B \rangle$ is the first moment of $P_{id}(B)$) and the Ginzburg–Landau parameter κ [13, 4, 32]. In order to estimate $\langle \Delta B^2 \rangle$ one often assumes that $P_{id}(B)$ is a sum of N Gaussian distributions (generally, $N = 1, 2, 3$) [33, 34]:

$$P_{id}(B) = \frac{\gamma_\mu}{\sqrt{2\pi}(A_1 + \cdots + A_N)} \times \sum_{i=1}^{N} \frac{A_i}{\sigma_i} \exp[(B - B_i)^2 / 2(\sigma_i/\gamma_\mu)^2], \tag{2}$$

where A_i, B_i, and σ_i/γ_μ are the weight factor, the first moment, and the standard deviation of the ith Gaussian component, respectively. $\gamma_\mu = 2\pi \times 135.5342$ MHz T^{-1} is the muon gyromagnetic ratio. The first and second moment of $P_{id}(B)$ are then readily obtained [33, 34]:

$$\langle B \rangle = \sum_{i=1}^{N} \frac{A_i\, B_i}{A_1 + \cdots + A_N}, \tag{3}$$

and

$$\langle \Delta B^2 \rangle = \sum_{i=1}^{N} \frac{A_i}{A_1 + \cdots + A_N} \left[(\sigma_i/\gamma_\mu)^2 + [B_i - \langle B \rangle]^2 \right]. \tag{4}$$

With modern computers it became possible to develop models that allow us to calculate $P_{\rm id}(B)$ for a FLL as a function of various parameters, such as magnetic penetration depth, coherence length, applied magnetic field, and FLL geometry (rectangular or hexagonal) [35, 17, 3, 4]. The London models (with different cut-off factors) provide the simplest and fastest way to calculate $P_{\rm id}(B)$ for the analysis of μSR data for $\kappa \gg 1$ [3]. Better approximations of $P_{\rm id}(B)$ for small values of κ and fields closer to B_{c2} can be obtained using the AGL model [16, 14]. Strictly speaking, Ginzburg–Landau theory is only valid in the neighborhood of the phase boundary $T_c(B)$ of a type-II superconductor. However, it is generally assumed that Ginzburg–Landau models are also good approximations for any field and temperature. The results obtained using the NGL model correspond to the minimum of the Ginzburg–Landau free energy, whereas other models described in this paper are just approximations to the NGL model. Therefore, the NGL model will be used as a reference for comparison with the AGL, ML, and LG models. A relatively simple method for calculating $P_{\rm id}(B)$ within the framework of the NGL model was proposed by Brandt [36, 4].

In the LG, ML, AGL, and NGL approximations the spatial distribution of the magnetic field in the mixed state of a type-II superconductor is described using the Fourier expansion:

$$B(\mathbf{r}) = \langle B \rangle \sum_{\mathbf{G}} \exp(-\mathrm{i}\mathbf{G}\mathbf{r})\, B_{\mathbf{G}}(\lambda, \xi). \tag{5}$$

Here, $\mathbf{r}$ is the vector coordinate in a plane perpendicular to the applied field. The origin of the coordinate system is in the center of a vortex core (see e.g. [29]), $\mathbf{G} = 4\pi/\sqrt{3}a(m\sqrt{3}/2, n + m/2)$ are the reciprocal lattice vectors for the hexagonal FLL, a is the intervortex distance, $B_{\mathbf{G}}$ are the Fourier components, and m, n are integer numbers. For the LG model the Fourier components $B_{\mathbf{G}}$ are [35, 3]

$$B_{\mathbf{G}} = \frac{\mathrm{e}^{-\xi^2 G^2/2}}{1 + G^2\lambda^2}. \tag{6}$$

For the ML model the Fourier components $B_{\mathbf{G}}$ are given by [17, 3]

$$B_{\mathbf{G}} = \frac{\mathrm{e}^{-\xi^2 G^2/2(1-b)}}{1 + G^2\lambda^2/(1-b)}, \tag{7}$$

For the AGL model the Fourier components $B_{\mathbf{G}}$ are [16, 14]

$$B_{\mathbf{G}} = \frac{\Phi_0}{S} \frac{f_\infty K_1[\frac{\xi_v}{\lambda}(f_\infty^2 + \lambda^2 G^2)^{1/2}]}{(f_\infty^2 + \lambda^2 G^2)^{1/2} K_1(\frac{\xi_v}{\lambda} f_\infty)}, \tag{8}$$

where $f_\infty = 1 - b^4$, and

$$\xi_v = \xi \left(\sqrt{2} - \frac{0.75}{\kappa} \right) (1 + b^4)^{1/2} [1 - 2b(1-b)^2]^{1/2}.$$

Here, $K_1(x)$ is the modified Bessel function. For applied magnetic fields $H \gg H_{c1}$ the relation $\mu_0 H \simeq \langle B \rangle$ holds [36]. Finally, for the NGL model no analytical solution for the Fourier components $B_{\mathbf{G}}$ exists. They are determined numerically [36, 4].

From the known spatial distribution of the magnetic field $B(\mathbf{r})$ in the mixed state one can extract the internal magnetic field distribution $P_{\rm id}(B)$ for the ideal FLL by means of the following equation:

$$P_{\rm id}(B) = \frac{\int \delta(B - B')\, \mathrm{d}A(B')}{\int \mathrm{d}A(B')}, \tag{9}$$

where $\mathrm{d}A(B')$ is the elementary area of the FLL with a field B' inside, and the integration is over a quarter of the FLL unit cell [29]. In order to take into account possible random deviations of the flux core positions from their ideal ones (vortex disorder) and/or possible broadening of the μSR spectra due to nuclear depolarization, one may convolute the ideal distribution $P_{\rm id}(B)$ with a Gaussian distribution [35]:

$$P(B) = \frac{1}{\sqrt{2\pi}\sigma_{\rm g}} \int P_{\rm id}(B') \exp\left[-\frac{1}{2} \left(\frac{B - B'}{\sigma_{\rm g}} \right)^2 \right] \mathrm{d}B', \tag{10}$$

where $\sigma_{\rm g}$ is the width of the Gaussian distribution. The relation between $\sigma_{\rm g}$, vortex disorder, and nuclear depolarization is described in section 3.4.

The μSR time spectra can be further simulated by performing the Fourier transform of $P(B)$ convoluted with the Gaussian function given in equation (10):

$$\tilde{P}(t) = A\mathrm{e}^{\mathrm{i}\phi} \int P(B)\mathrm{e}^{\mathrm{i}\gamma_\mu B t}\, \mathrm{d}B, \tag{11}$$

where A and ϕ are the initial asymmetry and the phase of the μSR time spectra, respectively. For the calculations of the spatial magnetic field distribution $B(\mathbf{r})$ in the FLL 31×31 Fourier components of the magnetic field and the reciprocal vector $\mathbf{G}$ were used. This allows one to calculate the second moment of $P(B)$ with a precision of better than 10^{-6}. The integral in equation (9) was calculated numerically over a quarter of the FLL unit cell, divided into approximately 100×100 equal pixels, depending on the mean magnetic field $\langle B \rangle$ (see figure 1 of [29]).

Equations (5)–(8) are only valid for isotropic superconductors or superconductors with axial symmetry with the external magnetic field applied along the symmetry axis. In the present study we mostly concentrate on the case of extreme type-II superconductors ($\kappa \gg 1$), such as the cuprate high temperature superconductors. Since the qualitative behavior of $P_{\rm id}(B)$ as a function of various parameters is essentially the same for a hexagonal and a square FFL, we will consider here only the hexagonal case.

In figure 1 we plot the spatial distribution of the magnetic field $B(\mathbf{r})$ in the mixed state and the corresponding local magnetic field distribution $P_{\rm id}(B)$ for $\lambda = 50$ nm, $\xi = 20$ nm, and $\langle B \rangle = 0.3B_{c2} \simeq 246.8$ mT, as determined by the NGL model. The ideal FLL has three characteristic fields: (i) the maximal field $B_{\rm max}$ corresponds to the field in the vortex core, (ii) the field at the peak of $P_{\rm id}(B)$ is the saddle point field $B_{\rm sad}$ (located in the middle between neighboring

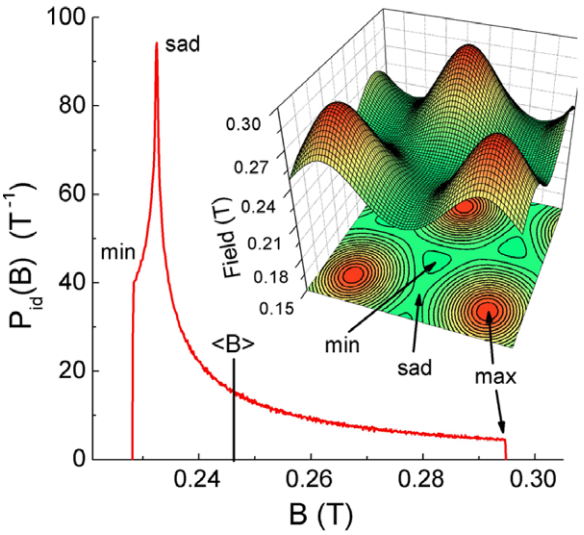

Figure 1. Example of a spatial distribution of the magnetic field $B(\mathbf{r})$ and the corresponding local magnetic field distribution $P_{\rm id}(B)$ for an ideal hexagonal FLL determined by the NGL method. The parameters used for the calculations are $\lambda = 50$ nm, $\xi = 20$ nm, and $\langle B\rangle = 0.3B_{c2} \simeq 246.8$ mT, and intervortex distance $a = 69.5$ nm.

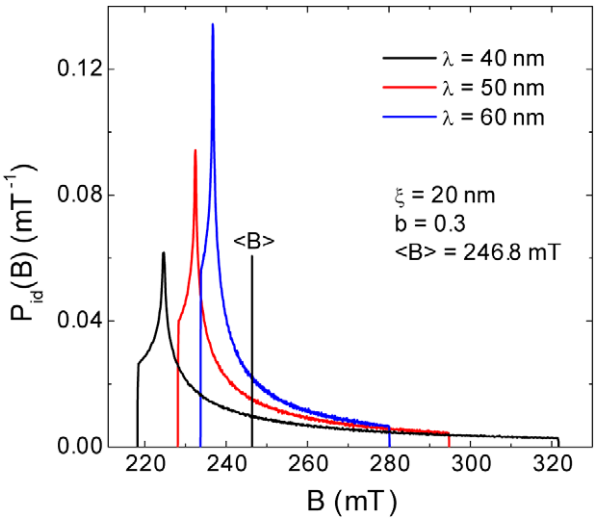

Figure 2. Local magnetic field distribution $P_{\rm id}(B)$ for an ideal hexagonal FLL obtained using the NGL model for different values of λ, at fixed ξ and applied field $B_{\rm app} \simeq \langle B\rangle$. The curves are normalized so that $\int P_{\rm id}(B)\,{\rm d}B = 1$. Note that the shape of $P_{\rm id}(B)$ strongly depends on λ.

vortices), and (iii) the minimal field $B_{\rm min}$ is in the center of the triangle of vortices forming the hexagonal FLL[4]. Instead of the full local magnetic field distribution $P_{\rm id}(B)$ we will use these characteristic fields to discuss the dependence of the shape of $P_{\rm id}(B)$ on different parameters.

3. Dependence of $P(B)$ on λ, ξ, $\langle B\rangle$, and $\sigma_{\rm g}$

In this section we concentrate on the analysis of the shape of $P(B)$ given in equation (10) as a function of penetration depth λ (section 3.1), coherence length ξ (section 3.2), mean magnetic field $\langle B\rangle$ (section 3.3), and Gaussian smearing width $\sigma_{\rm g}$ (section 3.4).

3.1. Dependence of $P_{id}(B)$ on λ

In figure 2 we show examples of the magnetic field distribution $P_{\rm id}(B)$ for different values of the magnetic penetration depth λ at constant mean field $\langle B\rangle = 0.3B_{c2} = 246.8$ mT and coherence length $\xi = 20$ nm, as calculated using the NGL model. The region between the minimal and the mean field $\langle B\rangle$ is most important, because the high field tail is usually below the noise level of experimental μSR spectra and is generally not observed, especially at low fields and for $\kappa \gg 1$. Our calculations show that the differences between the characteristic fields and the mean field $\langle B\rangle$ are proportional to $1/\lambda^2$. This is in full agreement with the results of Sidorenko *et al* [38] who obtained for applied fields $H_{c1} \ll H \ll H_{c2}$ and $\kappa \gg 1$ (in this case $\langle B\rangle \simeq \mu_0 H$) in the London approximation the following expressions:

$$\delta B_{\rm min} = B_{\rm min} - \langle B\rangle = -0.79(\Phi_0/4\pi\lambda^2)\ln 2, \qquad (12)$$

[4] At high fields and low temperatures the minimal and the saddle points are exchanged and the magnetic field distribution around the vortex core has a conical shape. See [37] and [35].

$$\delta B_{\rm sad} = B_{\rm sad} - \langle B\rangle = -\tfrac{2}{3}(\Phi_0/4\pi\lambda^2)\ln 2, \qquad (13)$$

$$\delta B_{\rm max} = B_{\rm max} - \langle B\rangle = 2(\Phi_0/4\pi\lambda^2)\ln\frac{a}{2\sqrt{2}K\xi}. \qquad (14)$$

Here, a is the intervortex distance, and $K = K(1/\sqrt{3}) \simeq 1.926$ is the complete elliptic integral of the first kind [38]. Hereafter, for convenience the quantities $\delta B_{\rm min}$, $\delta B_{\rm sad}$, and $\delta B_{\rm max}$ defined above are denoted as characteristic fields as well. From figure 2 and the pronounced dependence of the characteristic fields on $1/\lambda^2$ it is evident that the μSR time spectra strongly depend on λ. Therefore, it should be possible to extract reliable values of λ from experimental μSR data.

3.2. Dependence of $P_{id}(B)$ on ξ

Figure 3 shows the ξ dependence of the characteristic fields δB_α (α = min, sad, max) normalized to $\Phi_0/4\pi\lambda^2$ (cf equations (12)–(14)) for a set of different mean fields $\langle B\rangle$, as obtained using the LG model. All the characteristic fields δB_α disappear at $\xi \geqslant (\Phi_0/2\pi\langle B\rangle)^{1/2}$ (Φ_0 is the flux quantum), where superconductivity vanishes. Below a certain value of ξ the characteristic fields $\delta B_{\rm min}$ and $\delta B_{\rm sad}$ are independent of ξ, whereas $\delta B_{\rm max}$ still depends on ξ. However, in real μSR experiments $\delta B_{\rm max}$ cannot be determined out of the noise level at low $\langle B\rangle$. Therefore, at these low values of ξ μSR spectra are practically independent of ξ. In order to get a feeling for what this means for cuprate superconductors we assume $\xi \simeq 3$ nm, a typical value of ξ for cuprates below $T_c/2$. In this case the shape of $P_{\rm id}(B)$ is almost independent of ξ for fields $\langle B\rangle \leqslant 0.3$ T, where $\delta B_{\rm min}$ and $\delta B_{\rm sad}$ saturate (see figure 3). It is thus difficult to find the correct value of ξ at low magnetic fields. At higher fields the shape of $P_{\rm id}(B)$ strongly depends on ξ. Note that in figure 3 the curves corresponding to the smallest field ($\langle B\rangle = 0.01$ T) exhibit slightly smaller saturation values

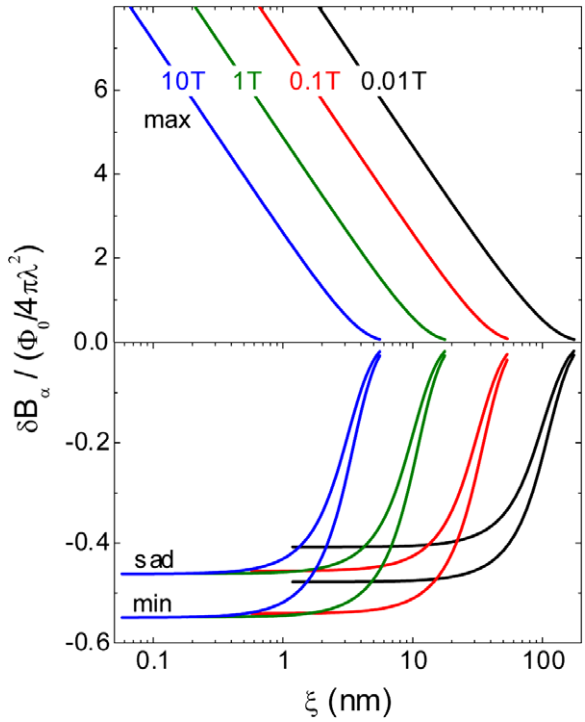

Figure 3. ξ dependence of the characteristic fields δB_α (α = min, sad, max) normalized to $\Phi_0/4\pi\lambda^2$ for a set of different applied magnetic fields ($B_{app} \simeq \langle B\rangle = 0.01$, 0.1, 1, 10 T) as obtained using the LG model. Note that there is a critical value of ξ below which δB_{min} and δB_{sad} are practically independent of ξ. This critical value depends on $\langle B\rangle$.

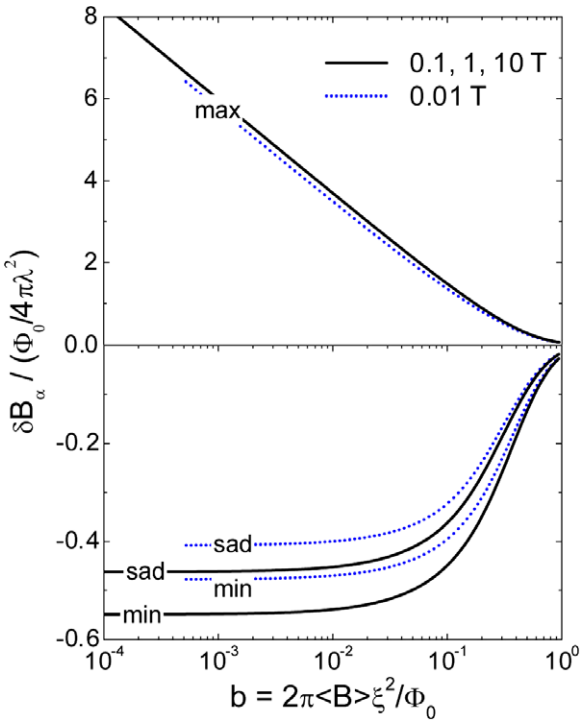

Figure 4. Characteristic fields δB_α (α = min, sad, max) of figure 3 plotted as a function of the reduced field $b = \langle B\rangle/B_{c2}(\xi)$ ($B_{c2}(\xi) = \Phi_0/2\pi\xi^2$) at $\langle B\rangle = 0.1$, 1, and 10 T (black solid line), and at 0.01 T (blue dotted line). Note that all the curves $\delta B_\alpha(\xi)$ of figure 3, at $\langle B\rangle = 0.1$, 1, 10 T merge to single curves $\delta B_\alpha(b)$.

of the characteristic fields δB_{min} and δB_{sad} than for the higher fields. The reason for this is discussed in section 3.3.

As shown by Brandt [36, 4] the ideal internal field distribution $P_{id}(B)$ may be expressed using normalized parameters, depending only on $\kappa = \lambda/\xi$ and $b = \langle B\rangle/B_{c2}$. In a similar way we can plot the curves in figure 3 not as a function of ξ, but as a function of $b = \langle B\rangle/B_{c2}$, where $B_{c2}(\xi) = \Phi_0/2\pi\xi^2$ (the relation obtained from Ginzburg–Landau theory). This plot is shown in figure 4. All the curves of figure 3, except the one for the smallest field $\langle B\rangle = 0.01$ T, fall on the same line.

3.3. Field dependence of $P_{id}(B)$

Before we discuss the dependence of the characteristic fields δB_α (α = min, sad, max) on various parameters, it is useful to define the minimal value of the reduced field $b_{min} = B_{c1}/B_{c2} \simeq \ln\kappa/2\kappa^2$ which is needed to form a regular FLL. This field corresponds to the limit below which the vortices can be considered as well separated and noninteracting.

Figure 5 shows δB_α (normalized to $\Phi_0/4\pi\lambda^2$) as a function of the reduced magnetic field b for different values of κ, as calculated using the LG model. The arrows at δB_{sad} correspond to $b_{min}(\kappa)$. This figure looks very similar to figure 4 and represents actually its generalization. It shows how δB_α depends on all three parameters λ, ξ, $\langle B\rangle$, and not only δB_α as a function of $\langle B\rangle$. Since figure 5 demonstrates the dependence of δB_α on all the parameters it is the basis of all further discussions. At high values of b, the characteristic fields $\delta B_\alpha(\langle B\rangle)$ and $\delta B_\alpha(\xi^2)$ coincide, but at lower fields they deviate substantially (dependence of δB_α on a parameter x means that all other parameters, except x, are fixed). The reason for this is obvious. For $b \to 0$ at constant ξ or B_{c2} the intervortex distance a increases, and $\langle B\rangle$, $\delta B_{min}(b)$, and $\delta B_{sad}(b)$ tend to zero as well. This is the reason for the smaller saturation values of δB_α at the lowest field $\langle B\rangle = 0.01$ T in figure 3. However, in the case of the ξ dependence, when $b \to 0$ at constant field $\langle B\rangle$, only the vortex core size is reduced, and the intervortex distance a does not change. This does not have much influence on the internal magnetic field distribution $P_{id}(B)$ for $\kappa \gg 1$ (see figure 5). When κ is reduced, the deviation of $\delta B_\alpha(\langle B\rangle)$ from $\delta B_\alpha(\langle B\rangle)_{\kappa=\infty}$ starts at higher values of b. For small values of κ the characteristic fields $\delta B_\alpha(\langle B\rangle)$ do not even reach saturated values as in the case of high κ and small b. Despite the similarity of $\delta B_\alpha(\langle B\rangle)$ and $\delta B_\alpha(\xi^2)$, the mean field $\langle B\rangle$ can easily be extracted from the fit (unlike ξ), since it defines the oscillation frequency of the μSR time spectrum.

3.4. Dependence of $P(B)$ on σ_g

In reality the internal magnetic field distribution in the mixed state of a type-II superconductor is influenced by several factors, which generally lead to an additional broadening of $P_{id}(B)$. (i) The FLL is never ideal, but disordered by random pinning effects of the vortex cores. (ii) For powder samples of anisotropic superconductors—such as the layered cuprate

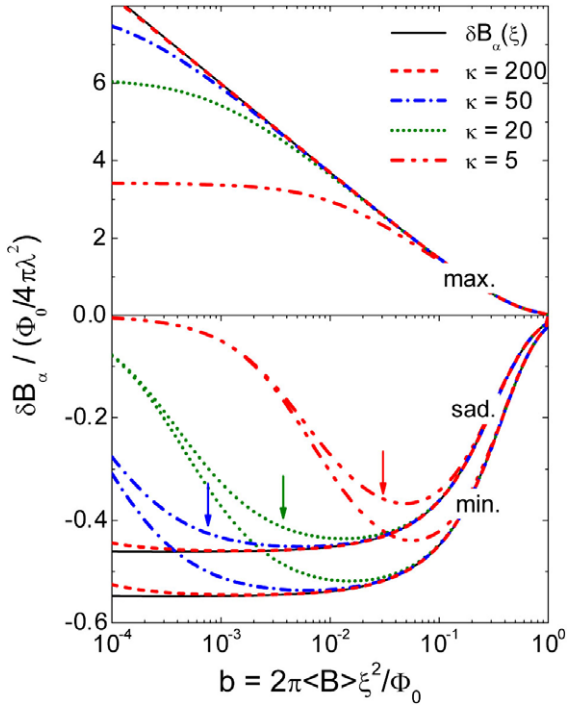

Figure 5. Characteristic fields δB_α (α = min, sad, max) calculated using the LG model as a function of the reduced field b (dashed, dotted and dash–dotted lines) for different values of κ. The black solid lines represent the curves $\delta B_\alpha(\xi)$ shown in figure 4 for $\langle B\rangle = 0.1$, 1, and 10 T. The arrows indicate the values of $b_{\min}$ at which $\langle B\rangle = B_{c1}$.

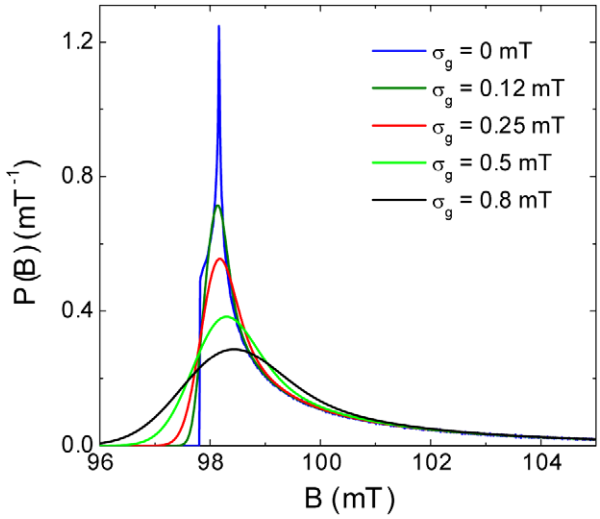

Figure 6. Change of the local magnetic field distribution $P_{id}(B)$ for an ideal FLL after convolution with a Gaussian distribution of various widths σ_g. The following parameters were used to generate $P_{id}(B)$ with the LG model: $\lambda = 200$ nm, $\xi = 4$ nm, and $\langle B\rangle = 100$ mT.

superconductors—the grains usually have random shapes, and therefore have anisotropic superconducting properties and demagnetization effects play a role [33]. (iii) The sample may contain magnetic nuclear moments or paramagnetic impurities. Vortex disorder and nuclear broadening can be taken into account by convoluting the ideal internal field distribution $P_{id}(B)$ with a Gaussian distribution of width (see equation (10)) [35, 17, 39]

$$\sigma_g = \sqrt{\sigma_{VD}^2 + \sigma_N^2}, \tag{15}$$

where σ_{VD} and σ_N are the contributions to the Gaussian broadening of $P_{id}(B)$ due to vortex disorder and nuclear depolarization, respectively[5]. For $\kappa \gg 1$ the standard deviation of the vortex core positions from the ideal positions in the FLL $\langle s^2\rangle^{1/2}$ is related to σ_{VD} by the following equation [17]:

$$\sigma_{VD} \propto \lambda^{-2}(1-b)\frac{\langle s^2\rangle^{1/2}}{a}. \tag{16}$$

Here $b = \langle B\rangle/B_{c2}$, and a is the intervortex distance.

Figure 6 shows examples of $P(B)$ for $\lambda = 200$ nm, $\xi = 4$ nm, $\langle B\rangle = 0.1$ T, and for various values of σ_g, calculated by means of the LG model. It is obvious that with increasing degree of disorder the Van Hove singularities in the ideal internal field distribution $P_{id}(B)$ are smeared out. Note that the low field part of $P_{id}(B)$ is mainly truncated by the Gaussian smearing, whereas the high field tail is nearly unaffected.

4. Comparison of different models

In this section the different models (LG, ML, AGL, and NGL) discussed in this work are compared. For this purpose the NGL model is used as a reference model for describing the mixed state of a type-II superconductor. In section 2 we showed that the characteristic fields δB_α for $\kappa \gg 1$ may be represented by single curves (see figure 5). Figure 7 shows the characteristic fields δB_α as a function of the reduced magnetic field $b = \langle B\rangle/B_{c2}$ in the limit of $\kappa \to \infty$ as calculated using the LG, ML, AGL, and NGL models. For small b values $\delta B_{\min}(b)$ and $\delta B_{sad}(b)$ coincide for all models. Deviations of the AGL and LG models from the NGL model appear above $b \approx 0.01$. Although the AGL and LG models may fit well the μSR spectra simulated using the NGL model, the fitted values of ξ may deviate substantially from the *real values* for reduced magnetic fields $b \gtrsim 10^{-2}$. This systematic deviation increases with increasing magnetic field. For the LG model, in contrast to the AGL model, the systematic errors even change sign with increasing magnetic field. One should note that for $\kappa > 5$ there is no advantage of using the AGL model instead of the LG model. Of all the models the ML model approximates best the NGL model up to about $b \simeq 0.1$, in agreement with previous results of Brandt [13]. However, at higher fields this model substantially deviates from the NGL model. The ML model has often been used to analyze experimental data for $b > 0.1$ [3, 29]. We found that μSR spectra simulated using the NGL model in the range $b = 0.1$–1 may well be fitted with the ML model. But for $b > 0.1$ the values of ξ extracted from the simulated μSR spectra are artificially reduced compared to the real values of ξ (see figure 7). For

[5] For powder samples with a Gaussian distribution of the first moments $\langle B\rangle$ due to Gaussian distribution of demagnetization factors N one may add an additional term $\sigma^2_{\langle B\rangle}$ to equation (15).

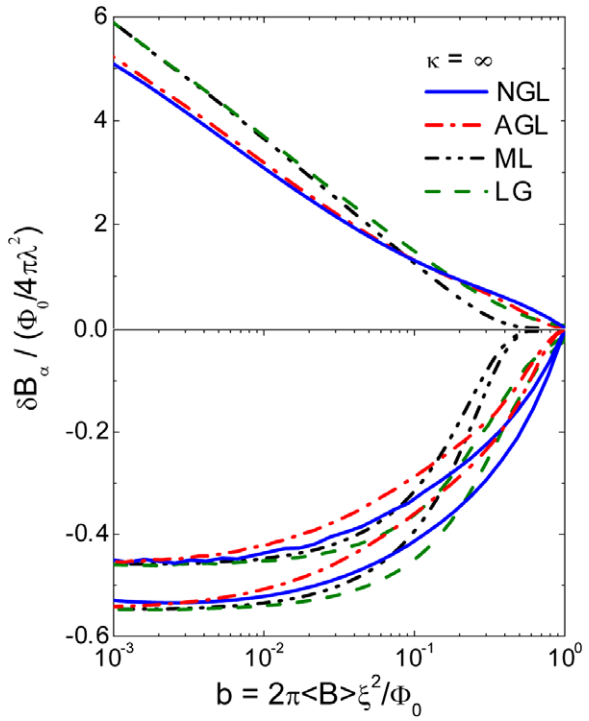

Figure 7. Characteristic fields δB_α (α = min, sad, max) as a function of the reduced field $b = 2\pi\langle B\rangle\xi^2/\Phi_0$ for $\kappa = \infty$, as calculated using the LG, ML, AGL, and NGL models.

smaller values of κ, the characteristic fields δB_α for the ML, AGL, and NGL models behave similarly to those of the LG model (see figure 5). Namely, for high reduced fields b all the curves with different values of κ coincide. The smaller κ, the higher the reduced field b when they start to deviate from the curves shown in figure 7. The only exception is for the AGL model, for which for $\kappa \leqslant 5$ the curves become closer to the NGL curves. Here we should mention that our results obtained with the NGL model are in full agreement with the calculations of Brandt [4].

5. Simulation and fitting of μSR spectra

In order to check the conclusions we reached in the previous sections 'experimentally', μSR time spectra with known parameters ($\langle B\rangle, \lambda, \xi, \sigma_g$) were simulated using the LG and NGL models. For the simulation of the μSR experiment a transverse field (TF) configuration with two positron detectors D1 and D2 located on opposite sides of the sample was used. The number of positrons detected by the detector D1 at time $t_i = i\Delta t$ is $N_1(t_i)\Delta t$ ($i = 1, 2, \ldots, 8000$; Δt was chosen to be 1.25 ns, corresponding to a typical time resolution for the GPS spectrometer at the Paul Scherrer Institute, Switzerland). This positron count number obeys Poisson statistics, and the standard deviation is simply given by $\sqrt{N_1(t_i)\Delta t}$. In the ideal case of no noise, the detector D1 would detect the signal $n_1(t_i) = n_0 e^{-t_i/\tau_\mu}[1 + P(t_i)]$, where n_0 is a constant depending on the number of muons detected (statistics) and the time interval Δt, $\tau_\mu = 2.197\,019(21)$ μs is the muon lifetime, and $P(t_i)$ is the noiseless μSR time signal (see equation (11)) to which noise has to be added. The signal monitored by detector D1 can be simulated using the equation $N_1(t_i) = n_1(t_i) + \sqrt{n_1(t_i)}g_i$, where g_i is a random number generator obeying Gaussian statistics with standard deviation and variance equal to 1. A similar signal but with opposite phase is registered by detector D2. In analogy to real μSR experiments one can calculate the asymmetry [1, 3] $A(t_i) = [N_1(t_i) - N_2(t_i)]/[N_1(t_i) + N_2(t_i)]$, yielding $P(t_i)$ with 'experimental noise'. The μSR time spectra were simulated according to the procedure described above with total statistics of 20 million events, a value typically used in real experiments.

The simulated μSR time spectra were then analyzed as follows.

(1) The μSR spectra simulated using the NGL model were analyzed by the second-moment (SM) method.
(2) The μSR spectra simulated using the LG model were analyzed using a fitting procedure based on the LG model.

According to the discussions in the previous sections the following important questions emerge.

(1) How reliable is the second moment obtained using a multi-Gaussian fit of the μSR spectra (see equation (17)) and the value of the penetration depth λ extracted from the second moment?
(2) Is there a correlation between σ_g and $1/\lambda^2$, since both of them influence the second moment of the μSR spectrum?
(3) Is it possible to extract reliable values of ξ from μSR spectra at low magnetic fields $b \simeq 10^{-3}$?
(4) Is there a correlation between λ and ξ at high fields (since for $b \approx 0.1$–0.9 both parameters strongly influence the characteristic fields δB_α)?

5.1. Test of the second-moment method

In this section the second-moment (SM) method is tested by analyzing μSR time spectra simulated using the NGL model with well defined parameters ($\langle B\rangle, \lambda, \xi, \sigma_g$). The SM method is theoretically well described in the literature [13, 38, 4] and was extensively used to extract the magnetic penetration depths of extreme type-II superconductors from μSR spectra [6–12]. In the framework of this method the μSR time spectra are usually fitted to a sum of N Gaussian components [33, 34]:

$$P(t) = \sum_{i=1}^{N} A_i \exp(-\sigma_i^2 t^2/2)\cos(\gamma_\mu B_i t + \phi). \qquad (17)$$

Here ϕ is initial phase of the muon beam, and A_i, σ_i, and B_i are the asymmetry, the relaxation rate, and the first moment of the ith Gaussian component, respectively. From the fit parameters A_i, σ_i, and B_i one readily obtains the first and the second moment of $P(B)$ from equations (3) and (4), respectively. Using equation (1) one finds the penetration depth λ. Here a serious question arises: How reliable is the value of λ obtained by the SM method using a multi-Gaussian fit? In order to investigate this question μSR time spectra were simulated using the NGL model for an extreme type-II superconductor (such as the cuprate superconductors) with a Ginzburg–Landau parameter $\kappa = 50 \gg 1$. The temperature dependence of λ was assumed to follow the relation (two-fluid

model) $\lambda(T)^{-2}/\lambda(0)^{-2} = [1-(T/T_c)^4]$ with $T_c = 22.5$ K and $\lambda(0) = 200$ nm (zero-temperature penetration depth). This approximately corresponds to the temperature dependence of λ in the strong-coupling BCS case [40]. In the first step we assume that there is no vortex disorder ($\sigma_{VD} = 0$) and no nuclear depolarization ($\sigma_N = 0$) present (cf equation (15)). The simulations were performed for three different magnetic fields: $\langle B\rangle = 0.05$, 0.5, and 5 T.[6] This corresponds to the reduced fields $b = 0.0024$, 0.024, and 0.24, an extremely small, an intermediate, and a high magnetic field, respectively (see figure 5). Since B_{c2} is decreasing with increasing temperature ($1/\xi^2 \propto B_{c2}$; $1/\xi^2 \propto 1/\lambda^2$ at constant κ), the analysis of the μSR spectra for $B = 5$ T makes sense only up to 21 K where $B_{c2}(21\text{ K}) \approx \langle B\rangle$ and superconductivity disappears. Noisy μSR time spectra were simulated using the parameters λ, ξ, and $\langle B\rangle$ as described above. For the technical parameters the following typical values were used: statistics 20×10^6, asymmetry $A = 0.2$, and phase $\phi = 0$.

For the analysis of the simulated μSR spectra, $P(t)$ in equation (17) was approximated by a sum of $N = 1, 2, 3, 4, 5$ Gaussians in order to check the reliability of the result obtained using a multi-Gaussian fit. The number of Gaussians N determines the quality of the fit. N should be increased from 1 until χ^2 (normalized to the degrees of freedom) is close to 1 within statistical scattering. The total asymmetry $A = \sum_{i=1}^{N} A_i$ and the phase ϕ of $P(t)$ in equation (17) were assumed to be known and were fixed in the fitting procedure. According to our experience, in order to reduce the scattering of the fitted values of the second moment, one should fix the asymmetries A_i of the individual Gaussians to their average values obtained using a fit with all parameters free. From the first and the second moments of the individual Gaussians one can calculate the second moment $\langle \Delta B^2\rangle$ of the μSR spectrum using equation (4), which corresponds to the second moment of $P_{id}(B)$ of an ideal FLL. The magnetic penetration depth λ is readily obtained from $\langle \Delta B^2\rangle$ with equation (1). The result of the analysis of the simulated μSR time spectra for an ideal FLL is shown in figure 8. For the 0.05 T data the finite value of $\kappa = 50$ was taken into account in the coefficient C in equation (1) [4]. One can see that the smaller the field, the greater the number of Gaussians N needed to describe the spectra. Whereas for 5 T $N = 2, 3$ Gaussians are sufficient for reproducing the spectra, $N = 4$ and $N = 5$ are required for 0.5 and 0.05 T, respectively. Note that the scattering of the data points increases with increasing number of Gaussians N. Although at 0.05 T the fitted values of $1/\lambda^2$ deviate systematically from the real values by a few per cent, the qualitative behavior of $1/\lambda^2(T)$ is the same. As will be shown below by adding a Gaussian smearing σ_g to the μSR spectra, the scattering is reduced, and a smaller number of Gaussians N are needed to describe the spectra. Figure 9 demonstrates how

[6] In a real μSR experiment with a time binning $\Delta t = 1.25$ ns the maximal possible field for a measurement is 2.95 T (this corresponds to two binnings per precession period). At higher fields the asymmetry of the signal drops. In our simulations, unlike in experiments, we do not integrate the positron counts within the time interval Δt, but simulate the detector counts at $t_i = i\Delta t$. For this reason it is possible to simulate and fit μSR data at higher fields due to the stroboscopic effect. In this case the absolute value of the real field is the fitted field plus $N \times 2.95$ T, where N is a positive integer number.

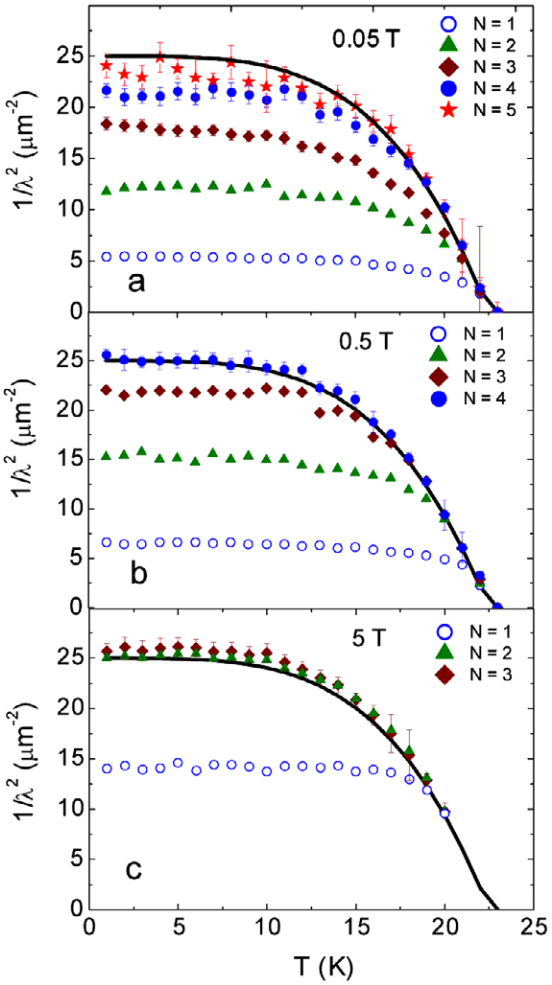

Figure 8. Fit results for λ^{-2} obtained by the second-moment method. The noisy spectra for the three different fields of 0.05, 0.5, and 5 T were simulated using the NGL method for an ideal FLL as described in the text, and then analyzed using a multi-Gaussian function with different number of Gaussians ($N = 1, 2, 3, 4, 5$) as defined in equation (17). The black solid lines correspond to the real values of λ^{-2} used for the simulation.

the local magnetic field distribution $P_{id}(B)$ for an ideal FLL can be approximated by $N = 5$ Gaussians. Although not all the details of $P_{id}(B)$ are reproduced, the overall agreement is good, in particular the second moment.

In order to test the second-moment method under more realistic conditions one should add a Gaussian smearing σ_g to the μSR spectra (cf equation (10)). According to equation (15), we assume for the further discussions that σ_g is composed of two components: $\sigma_g = (\sigma_{VD}^2 + \sigma_N^2)^{1/2}$, where σ_{VD} denotes the temperature dependent smearing due to vortex disorder, and σ_N is the temperature independent smearing due to nuclear depolarization (cf equation (16)). For a constant vortex disorder $\langle s^2\rangle^{1/2}/a = \text{const.}$ (rigid vortex lattice) and reduced field b, the relation $\sigma_{VD} \propto 1/\lambda^2$ holds. As is obvious from equation (16), for $\langle B\rangle = 5$ T the term $(1-b) = 0.76$ substantially deviates from unity and has to be taken into account in the simulation of μSR data.

For the simulations of the smeared μSR spectra the following values for single-crystal $La_{1.83}Sr_{0.17}CuO_{4-\delta}$ were

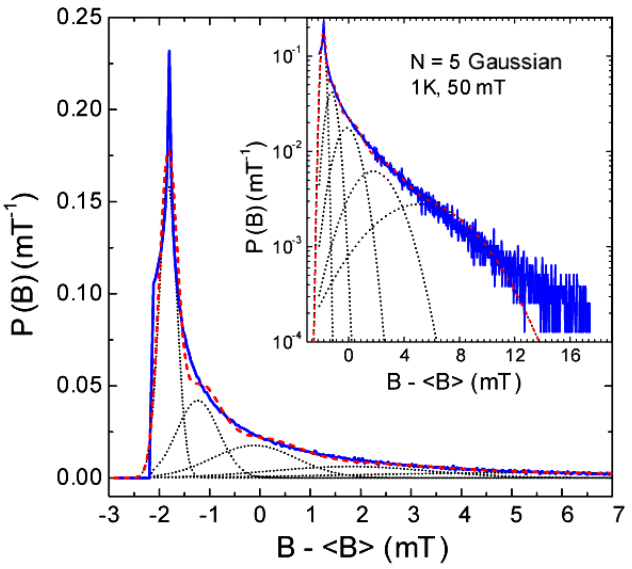

Figure 9. Comparison of the ideal field distribution $P_{id}(B)$ simulated using the NGL model at 0.5 T and 1 K (blue solid line) with $P(B)$ obtained using a Gaussian fit with $N = 5$ (red dashed line). The five individual Gaussian components used for the fit are also shown (black dotted lines). The inset shows the same plot but on a semi-logarithmic scale.

used: $\sigma_{VD} = \beta/\lambda^2$, $\beta = 2.585 \times 10^4$ (mT nm^2) and $\sigma_N = \sigma_{Cu} = 0.27$ mT [41]. Noisy μSR time spectra were simulated using the parameters λ, ξ, $\langle B \rangle$, and σ_g as described above. For the technical parameters the following typical values were used: statistics 20×10^6, asymmetry $A = 0.2$, and phase $\phi = 0$.

The total second moment $\langle \Delta B^2 \rangle_t$ of a μSR spectrum with Gaussian smearing σ_g obtained using a multi-Gaussian fit contains three components:

$$\langle \Delta B^2 \rangle_t = \langle \Delta B^2 \rangle + \sigma_{VD}^2 + \sigma_N^2, \tag{18}$$

where $\langle \Delta B^2 \rangle$, σ_{VD}^2, and σ_N^2 are the second moments due to the internal field variation in the ideal FLL, the vortex disorder, and the nuclear depolarization, respectively. In order to obtain λ from the total second moment measured in real experiments one determines σ_N above T_c, and assumes that $\sigma_{VD}^2 \ll \langle \Delta B^2 \rangle$ in equation (18), i.e. $\langle \Delta B^2 \rangle_t \simeq \langle \Delta B^2 \rangle + \sigma_N^2$ [42]. From the first and the second moments of the individual Gaussians one can calculate the total second moment $\langle \Delta B^2 \rangle_t$ of the μSR spectrum using equation (4) (note that in equation (4) $\langle \Delta B^2 \rangle$ has to be replaced by $\langle \Delta B^2 \rangle_t$ for the case $\sigma_g \neq 0$). By means of equations (18) and (1) the magnetic penetration depth λ then is readily obtained. Figure 10 shows the results for the penetration depth obtained by the second-moment method with $N = 1, 2, 3, 4$ Gaussians. Note that a single Gaussian does not give reliable results in agreement with earlier findings [33]. However, with increasing number of Gaussians N the quality of the fits substantially improves. In order to fit the simulated data at 0.05 T at least three or, better, four Gaussians are required. For $N = 3$ there is a systematic deviation of about 10% of λ^{-2} from the real value (or 5% for λ), whereas for $N = 4$ the values of λ^{-2} are scattered within a few per cent around

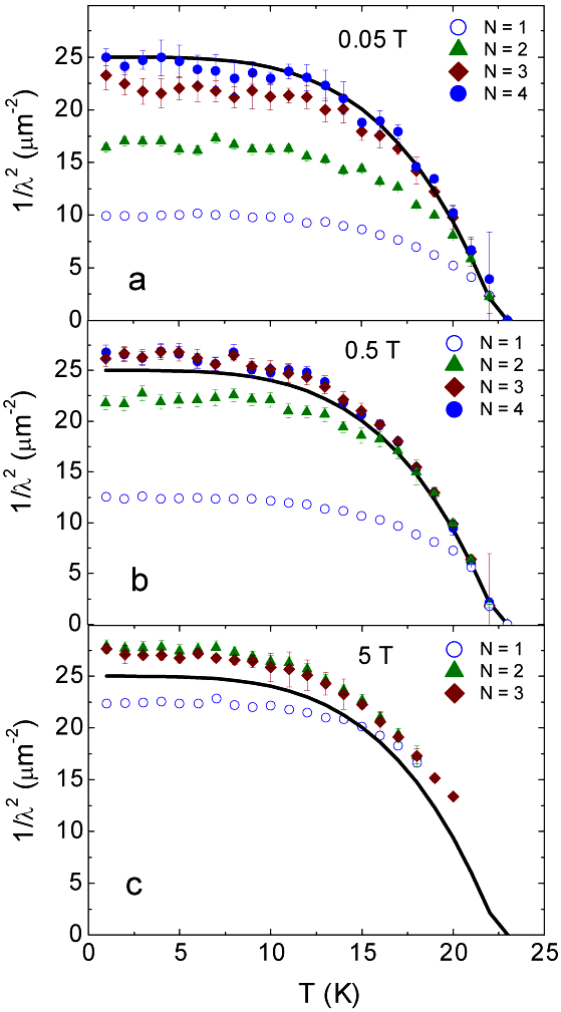

Figure 10. Fit results for λ^{-2} obtained by the second-moment method. The noisy spectra for the three different fields of 0.05, 0.5, and 5 T were simulated using the NGL method including Gaussian smearing σ_g as described in the text, and then analyzed using a multi-Gaussian function with different numbers of Gaussians ($N = 1, 2, 3, 4$), as defined in equation (17). The black solid lines correspond to the real values of λ^{-2} used for the simulation.

the real ones. For the data simulated at 0.5 T even $N = 3$ Gaussians are sufficient for describing the local magnetic field distribution $P(B)$, and the values of λ^{-2} are systematically shifted only within a few per cent. Figure 11 shows an example of a real internal field distribution $P(B)$ ($\langle B \rangle = 0.5$ T, $T = 1$ K of figure 10) and the reconstructed $P(B)$ obtained from the analysis of the simulated μSR spectrum (2×10^7 statistics) using a Gaussian fit with $N = 3$. It is obvious that three Gaussians describe well the shape of the real $P(B)$. The largest systematic error in λ^{-2} obtained using a multi-Gaussian fit is observed at 5 T ($b = 0.24$). At such a high field ($\langle B \rangle \simeq B_{c2}/4$) the variation of the internal field is relatively small (see figure 7), and the Gaussian smearing σ_{VD} (cf equation (18)) due to vortex disorder becomes essential. The second moment of this Gaussian smearing cannot be neglected and considerably contributes to the total second moment $\langle \Delta B^2 \rangle_t$ of $P(B)$. This leads to systematically higher values of λ^{-2} obtained using multi-Gaussian fits at high magnetic fields. Note, however,

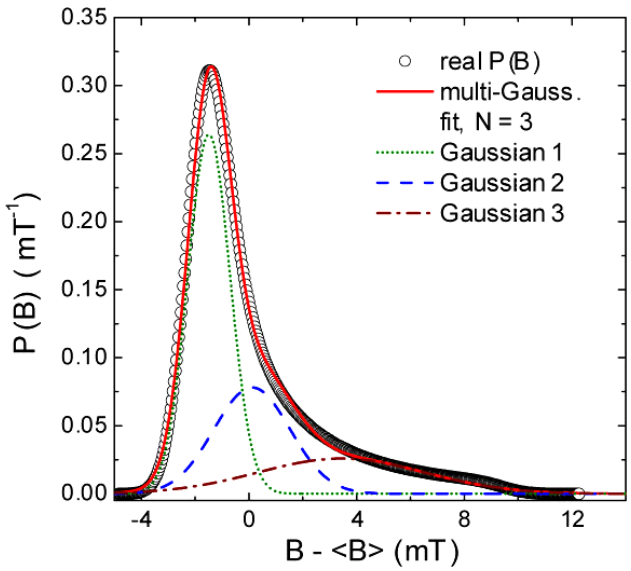

Figure 11. Comparison of the real field distribution $P(B)$ (empty circles) simulated using the NGL model for parameters $\lambda = 200$ nm, $\xi = 4$ nm, $\langle B\rangle = 0.5$ T, $\sigma_g = 0.7$ mT (the data point at $T = 1$ K for $N = 3$ in figure 10(b)) with $P(B)$ obtained using a Gaussian fit with $N = 3$ (red solid line). The dotted, dashed, and dash–dotted lines represent individual Gaussian components used for the fit. It is obvious that a multi-Gaussian fit may well describe the real $P(B)$.

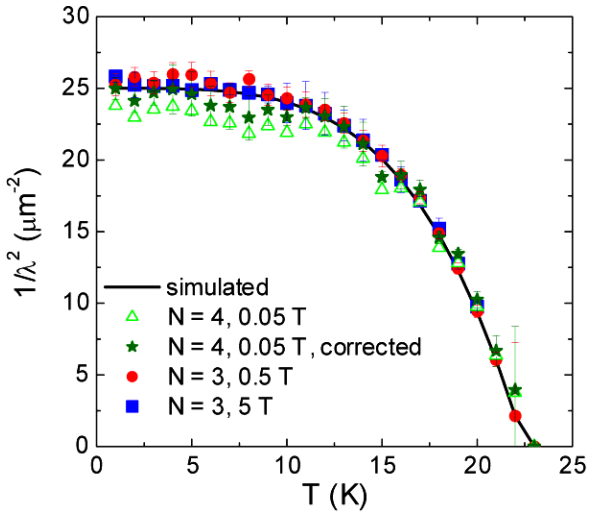

Figure 12. Temperature dependence of $1/\lambda^2$ determined from $\langle\Delta B^2\rangle$, assuming that σ_{VD} is known as described in the text. Triangles: $N = 4$, 0.05 T; stars: $N = 4$, 0.05 T, corrected for finite $\kappa = 50$ (see the text for an explanation); circles: $N = 3$, 0.5 T; squares: $N = 3$, 5 T.

that there are two reasons why the contribution to the second moment due to vortex disorder is reduced with increasing magnetic field, and consequently the systematic error in λ^{-2}. (1) At high fields $\sigma_{VD} \propto (1 - b)$ (cf equation (16)), which was taken into account in the simulations of the μSR spectra. (2) Vortex disorder, $\langle s^2\rangle^{1/2}/a$, is expected to decrease with increasing magnetic field, because of the strong repulsive interaction between the vortices at high fields (see e.g. [4]).

By means of a multi-Gaussian fit it is not possible to separate $\langle\Delta B^2\rangle$ and σ_{VD} from the measured total second moment $\langle\Delta B^2\rangle_t$ (cf equation (18)). Assuming that $\sigma_{VD} = 0$ yields a lower limit for λ (upper limit for $1/\lambda^2$), as clearly demonstrated in figures 10(b) and (c) where the values of $1/\lambda^2$ are systematically too large. It is interesting to investigate what the values of $1/\lambda^2$ are after correction with the real value of σ_{VD}. For this purpose we write equation (16) in the form $\sigma_{VD} = \beta\lambda^{-2}$ and with the help of equations (1) and (18) we obtain

$$\lambda^{-2} = [C/(1+\epsilon)]^{1/2}[\langle\Delta B^2\rangle_t - \sigma_N^2]^{1/2}, \qquad (19)$$

where $\epsilon = C\beta^2$ is the correction due to vortex disorder. The values of $1/\lambda^2$ plotted in figure 10 were obtained with $\epsilon = 0$ (no vortex disorder correction). Figure 12 shows some of the results of figure 10 after correcting the values of $1/\lambda^2$ with the values of $\epsilon_{T=0} = 0.050$, 0.073, and 0.155 for 0.05 T, 0.5 T, and 5 T, respectively (ϵ is temperature dependent, since $C(b(T), \kappa)$ is temperature dependent). The corrected values of $1/\lambda^2$ are in good agreement with the real values (solid line in figure 12), except for the data at 0.05 T where a systematic deviation of about 5–10% is observed. One of the reasons for this deviation is that $\kappa = 50$ used in the simulations is not infinite. This implies that at 0.05 T ($b \simeq 0.0024$) the parameter $C^{-1/2}$ in equations (1) and (19) is about 5% smaller [4]. The stars in figure 12 represent the corrected values of $1/\lambda^2$ at 0.05 T, which are only about 3% systematically lower than the real values.

5.2. Test of the London model with Gaussian cut-off (LG)

In order to test the reliability of the advanced methods described in section 2 we first simulated noisy μSR spectra and then fitted them like with the second-moment method. To avoid systematic errors in the fit results it is important to analyze the data using the same model as they were simulated. Here we present results for the LG model, since it can approximate experimental data well over the whole field range (see figure 7). Similar results are also obtained with all other models. The temperature dependence of the penetration depth λ was assumed to follow the relation $\lambda^{-2}(T)/\lambda^{-2}(0) = [1 - (T/T_c)^2]$ with $\lambda(0) = 200$ nm and $T_c = 22.5$ K. The Ginzburg–Landau parameter $\kappa = 50$, and Gaussian smearing $\sigma_g(T) = (\sigma_{VD}^2(T) + \sigma_N^2)^{1/2}$ [$\sigma_{VD} \propto 1/\lambda^2(T)$] was chosen, to be the same as in section 5.1. Again the μSR spectra were simulated for three different mean fields $\langle B\rangle = 0.05$, 0.5, and 5 T ($b = 0.0024$, 0.024, 0.24). As before the mean field was assumed to be temperature independent. The statistics, asymmetry, and phase of the μSR time spectra were chosen to be 20×10^6, 0.2, and 0, respectively.

The results of the fits of the simulated μSR spectra with all the parameters free (except A and ϕ) are shown in figure 13. Phase ϕ and asymmetry A were assumed to be known and were fixed to their real values. In order to exclude any artificial influence on the fitting procedure we performed the fits in automatic mode. This means that with increasing temperature the fit results for temperature T_i were used as initial parameters for the next temperature T_{i+1}. For T_1 (lowest temperature) the

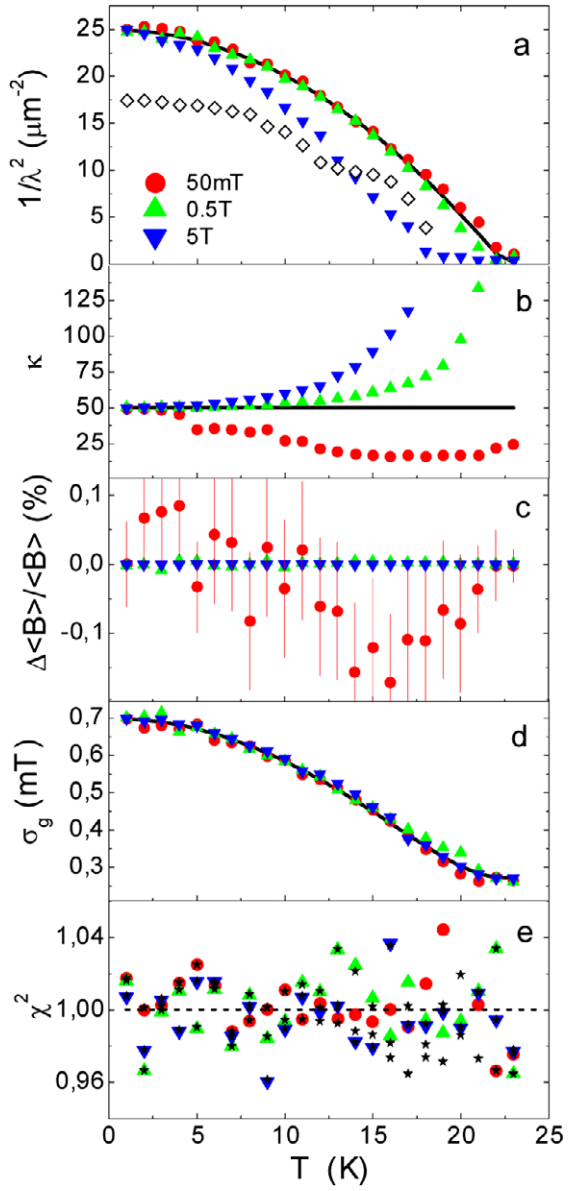

Figure 13. Summary of the fit results for the μSR spectra simulated using the LG model. The fitted values $1/\lambda^2$, κ, $\Delta\langle B\rangle/\langle B\rangle$, and σ_g, as well as χ^2, are plotted as a function of temperature T for three different fields 0.05 T (circles), 0.5 T (upward-pointing triangles), and 5 T (downward-pointing triangles) for 20 million statistics. The parameters $1/\lambda^2$, κ, $\Delta\langle B\rangle/\langle B\rangle$, and σ_g were free during the fitting procedure. The solid lines correspond to the true values of the parameters. $\Delta\langle B\rangle/\langle B\rangle = (\langle B\rangle_{\rm fit} - \langle B\rangle_{\rm real})/\langle B\rangle_{\rm real}$ denotes the relative deviation of the fitted value $\langle B\rangle_{\rm fit}$ from the real $\langle B\rangle_{\rm real}$. For comparison χ^2 was also determined for the real values of the parameters (black stars). The black empty diamonds in (a) show a possible fit result for $1/\lambda^2$ at 5 T with extremely wrong initial parameters. Note that the error bars of $1/\lambda^2$, as calculated using the fitting program (the function 'fit' of the MATLAB program was used), are within the point size ($\simeq$2%).

correct initial parameters were used. As shown in figure 13 for λ^{-2} we got good results at low fields; however there are substantial systematic deviations for κ. At the highest field there are substantial systematic deviations of the fitted values for both λ and κ, although the goodness of fit χ^2 for

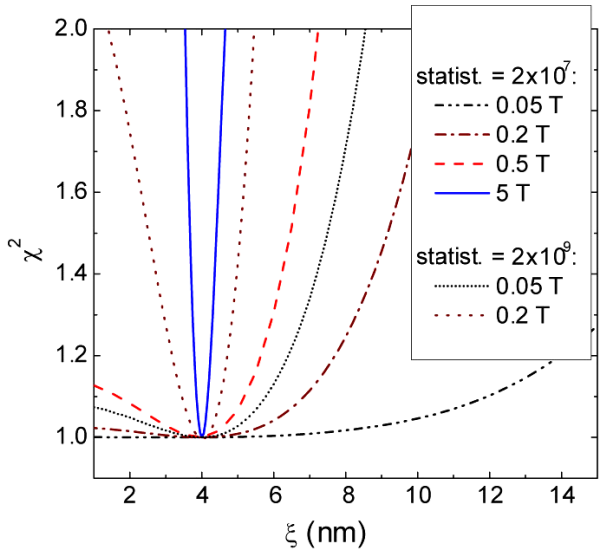

Figure 14. χ^2 as a function of ξ for the μSR spectra simulated using the LG model with 20 million counts, $\langle B\rangle = 0.05$, 0.2, 0.5, and 5 T, $\lambda = 200$ nm, $\xi = 4$ nm, and $\sigma_g = 0.7$ mT. For comparison $\chi^2(\xi)$ is also shown for the higher statistics of 2000 million at $\langle B\rangle = 0.05$ and 0.2 T. The statistically scattered minimal value of χ^2 was normalized to 1. Note that the dependence of χ^2 on ξ at low fields is weak.

these fits is comparable to those for the correct parameters (figure 13). The values of χ^2 weighted and normalized to the degrees of freedom ($\approx$8000) scatter around 1 within 0.04, as expected for the present degrees of freedom. The black stars in figure 13 denote χ^2 for the true values of the parameters for comparison. From all the fitted parameters, the values obtained for κ deviate most from the real ones for all the fields. In order to check the reason for this strong deviation for κ at 0.05 T, the fit was performed using different initial parameters. For λ, $\langle B\rangle$, and σ_g correct values within a few per cent were obtained, whereas ξ was found to be in the range 2–13 nm with a very good value of χ^2. The dependence of χ^2 on ξ for different fields and statistics is demonstrated in figure 14. It is evident that at low fields and 20 million statistics the quality of the fit is practically independent of ξ over a very broad range. For the 5 T data not only κ but also λ substantially deviates from the real value (see figure 13). The good agreement at low temperatures is misleading, since it is only due to the correct initial parameters that we set for the lowest temperature. The empty black diamonds in figure 13(a) show the fit result for intentionally extremely wrong starting parameters. In real measurements one never knows the optimal starting parameters. We performed fits of the 5 T data at $T = 1$ K with different starting values of λ, ξ, $\langle B\rangle$, and σ_g. It was found that for $\langle B\rangle$ and σ_g one obtains values close to the real ones; however, for λ and ξ this is not the case. Figure 15 shows the variation of the values of λ and ξ during the fitting process. The starting values of λ and ξ are indicated by number $\boxed{1}$. The numbers $\boxed{2}$, $\boxed{3}$, ..., $\boxed{10}$ indicate the values of λ and ξ after each five fitting iterations. The maximal number of fitting iterations was not restricted. However, 50 iterations were usually sufficient, and the fit was terminated when the relative changes of all the parameters during the iteration were

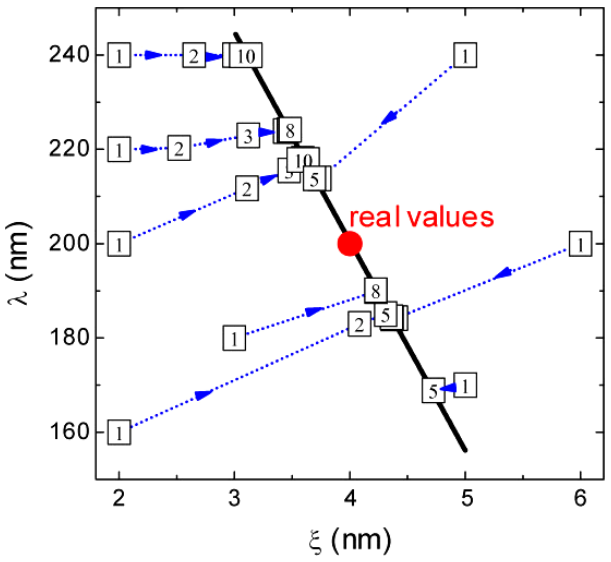

Figure 15. Visualization of the fitting process of the simulated μSR spectrum for the parameters $\lambda = 200$ nm, $\xi = 4$ nm, $\langle B \rangle = 5$ T, $\sigma_g = 0.7$ mT using the LG model. Number [1] indicates the starting values for λ and ξ. The numbers [2], [3], ..., [10] denote the values of λ and ξ after each five iterations of the fitting process. The fit was terminated when relative changes of all the parameters were less than 10^{-6}. The solid line shows the points in the λ versus ξ plane where the fit is finally converging. Note that the fit results for the other parameters $\langle B \rangle$ and σ_g are close to the real ones, independently of the starting values.

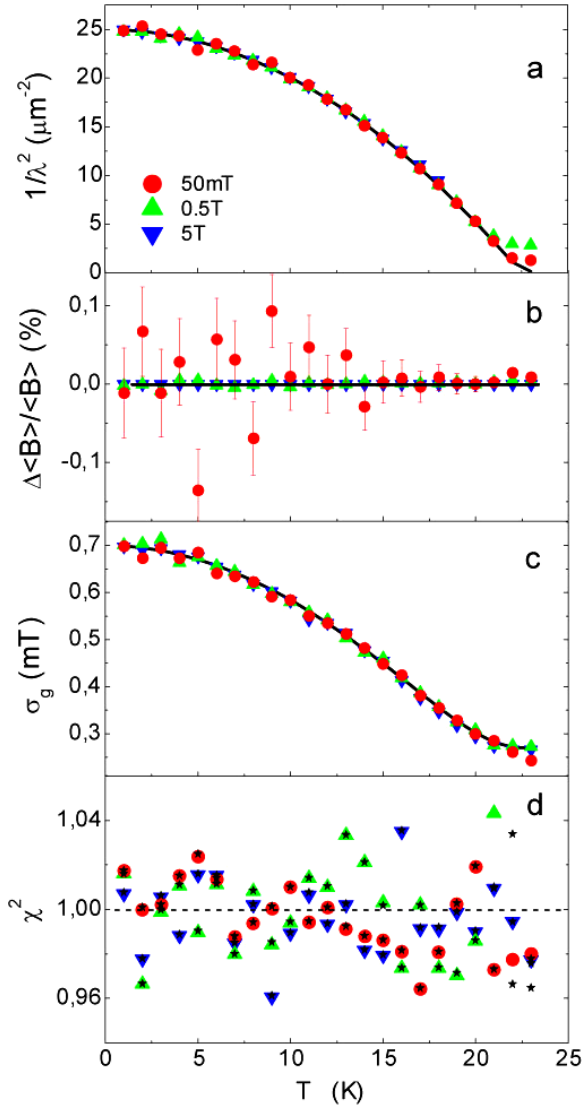

Figure 16. Summary of the fit results for the μSR spectra simulated using the LG model. The fitted values $1/\lambda^2$, $\Delta\langle B \rangle/\langle B \rangle$, and σ_g, as well as χ^2, are plotted as a function of temperature T for three different fields 0.05 T (circles), 0.5 T (upward-pointing triangles), and 5 T (downward-pointing triangles) for 20 million statistics. The parameters $1/\lambda^2$, $\Delta\langle B \rangle/\langle B \rangle$, and σ_g were free during the fitting procedure, whereas κ was fixed at the real value. The solid lines correspond to the true values of the parameters. $\Delta\langle B \rangle/\langle B \rangle = (\langle B \rangle_{fit} - \langle B \rangle_{real})/\langle B \rangle_{real}$ is the relative deviation of the fitted value $\langle B \rangle_{fit}$ from the real one $\langle B \rangle_{real}$. For comparison χ^2 was also determined for the real values of the parameters (black stars).

less than 10^{-6}. The final results of the fit eventually correspond to local minima of χ^2. The fit converges on a certain $\lambda = \lambda(\xi)$ curve denoted by the black line in figure 15, indicating a possible correlation between λ and ξ at high fields. Therefore, we can conclude that the determination of a reliable value of ξ is problematic at low fields as expected (see figure 3). At higher fields not only the value of ξ, but also the value of λ may systematically deviate from the real value. However, at low fields reliable values of $\langle B \rangle$, σ_g, and λ may presumably be well determined from fits with the advanced models.

The next step for improving the fitting procedure is to restrict some parameters. On the basis of the results obtained from the free parameter fits we conclude that a good candidate for restriction is ξ, especially at low fields. One can fix κ in order to relate ξ to λ via $\xi = \lambda/\kappa$ and let the other parameters λ, $\langle B \rangle$, and σ_g be free. This is also reasonable from a theoretical point of view. In the BSC approximation κ does not change substantially with temperature in the weak-coupling limit [43]. The results of the fits with the only restricted parameter κ (i.e., ξ was calculated with $\xi = \lambda/\kappa$) are shown in figure 16. It is obvious that the fits are excellent and all the parameters are very close to the real ones with only small statistical scattering.

5.3. Correlation between σ_g and λ^{-2} for small values of b

As shown in figure 6, with increasing Gaussian smearing σ_g the characteristic fields of the internal magnetic field distribution $P_{id}(B)$ of the ideal FLL are gradually washed out, and $P(B)$ tends to become an asymmetric Gaussian-like distribution. Therefore, one expects some correlation between σ_g and the inverse square of the penetration depth $1/\lambda^2$, since both of them influence the second moment of the μSR spectrum. In order to show the possibility of extracting the real values of λ and σ_g from μSR spectra, we simulated μSR data using the ML model and then calculated the goodness of fit χ^2 as a function of λ and σ_g with the other parameters fixed to their true values. Figure 17(a) shows χ^2 as a function of λ with the other parameters fixed to their true values. For the simulated data the following parameters were used: $\lambda_0 = 200$ nm,

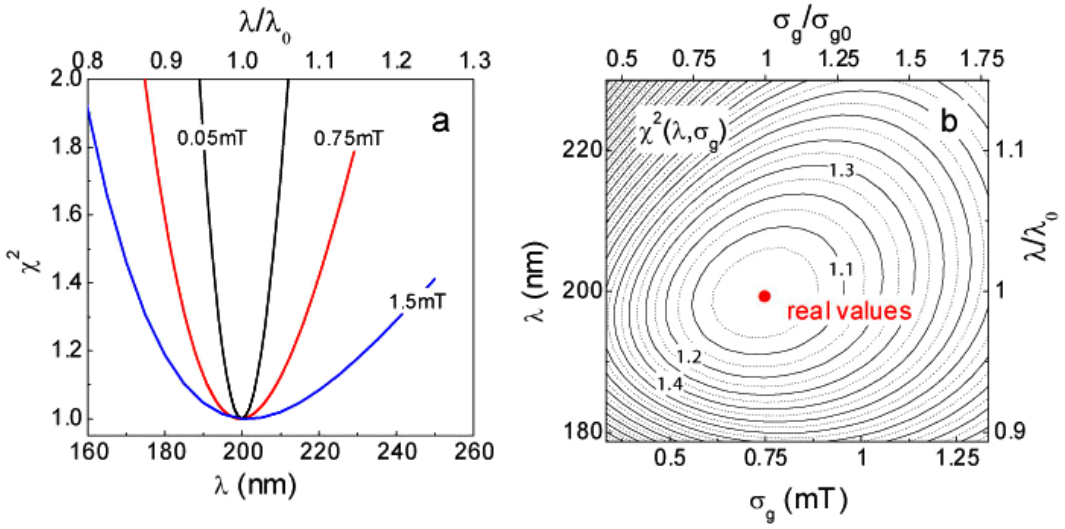

Figure 17. (a) χ^2 as a function of λ with the other parameters set to the true values. The following parameters were used for the μSR data simulation: $\lambda_0 = 200$ nm, $\xi_0 = 1$ nm, $b_0 = 10^{-3}$, 20 million statistics, and $\sigma_{g0} = 0.05$, 0.75, and 1.5 mT. (b) Contour plot of χ^2 as a function of λ and σ_g for the data simulated using $\lambda_0 = 200$ nm, $\xi_0 = 1$ nm, $b_0 = 10^{-3}$, $\sigma_{g0} = 0.75$, and 20 million counts (red point). In both figures the ML model was used for the calculations, and the statistically scattered minimal value of the χ^2 was normalized to 1. The real values of λ and ξ are indicated by the red point.

$\xi_0 = 1$ nm, $b_0 = 10^{-3}$, $\sigma_{g0} = 0.05$, 0.75, 1.5 mT, and 20 million counts. It is evident that with increasing σ_{g0} the error of λ extracted from the fit increases. Figure 17(b) shows a contour plot of χ^2 as a function of λ and σ_g calculated for data with $\lambda_0 = 200$ nm, $\xi_0 = 1$ nm, $b_0 = 10^{-3}$, $\sigma_{g0} = 0.75$, and 20 million statistics. This approximately corresponds to the case that we analyzed before. From the figure we conclude that λ^{-2} and σ_g are slightly correlated, but it is possible to extract them simultaneously if ξ is fixed. This agrees well with the results of the analysis performed in section 5.2.

5.4. Correlation between ξ and λ

For low magnetic fields the dependence of the μSR spectrum on the coherence length ξ is very weak (see figure 14). But with field increasing towards B_{c2} the shape of the spectrum becomes dependent not only on the penetration depth λ, but also on ξ (see figure 7). An increase of λ and/or ξ causes a decrease of the second moment and the characteristic fields. Therefore, it is expected that a decrease of λ is correlated with an increase of ξ in the fitting procedure and vice versa. So far, to our knowledge, this problem has been discussed previously only by Riseman *et al* [17]. Here we study this problem in more detail. For this procedure we determined χ^2 for simulated μSR data as a function of λ and ξ at fixed $\langle B\rangle_0 = 0.5B_{c2}$ and Gaussian smearing $\sigma_{g0} = 0.5$ mT. We have chosen the case of a relatively small $\kappa_0 = 2.5$ ($\lambda_0 = 50$ nm and $\xi_0 = 20$ nm) for the data simulation, since the relative volume of the vortex cores is large, and therefore it is easier to extract ξ from the fits. As before, the statistics were 20×10^6. The result of the analysis with the NGL model is shown in figure 18, where a contour plot of χ^2 as a function of λ and ξ with the other parameters fixed is displayed. There is indeed a strong correlation between λ and ξ. For $\lambda(\xi) \approx 58.68 + 2.14\xi - 0.127\xi^2$, where $\chi^2 \simeq 1$ is minimal, the fits converge after a few hundred iterations.

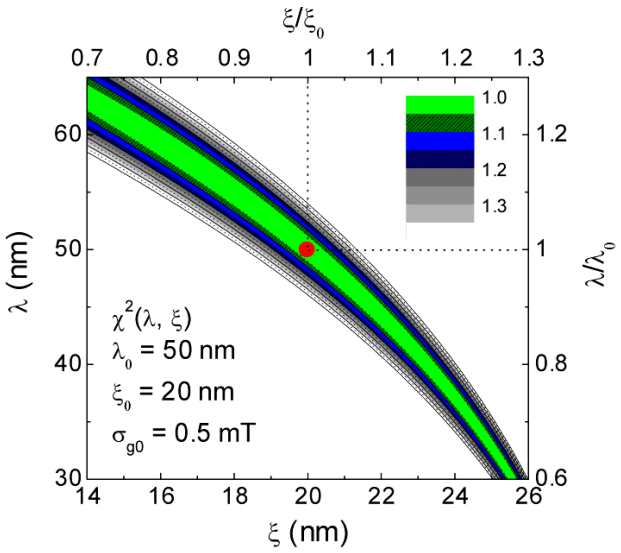

Figure 18. Contour plot of χ^2 as a function of λ and ξ for the data simulated using parameters $\lambda_0 = 50$ nm, $\xi_0 = 20$ nm, $b_0 = 0.5$, $\sigma_{g0} = 0.5$ mT, and 20 million counts, calculated using the NGL model. The fitted parameters λ and ξ exhibit a strong correlation, which is the reason for the pronounced systematic deviations of the fitted values of λ^{-2} and κ at 5 T from the real values displayed in figure 13. The statistically scattered minimal value of χ^2 is normalized to 1. The real values of λ and ξ are indicated by the red point.

Tests showed that for different starting parameters the fits were converging in the correlated region of $\xi = 14$–24 nm and $\lambda \approx 36$–63 nm. This region lies within the interval of $\chi^2 < 1.05$ (see figure 18). It should be noted that for such a high reduced field $b = 0.5$ as was used here for the analysis, the qualitative dependences of the characteristic fields δB_α on λ, ξ, and $\langle B\rangle$ are independent of $\kappa = \lambda/\xi$ (see figure 5). Therefore the

qualitative behavior of the contour plot of $\chi^2(\lambda/\lambda_0, \xi/\xi_0)$ in figure 18 is independent of $\kappa_0 = \lambda_0/\xi_0$ for any $\kappa_0 > 5$.

The situation could be improved for fields $b \simeq 10^{-2}$ where the minimal and saddle point fields slightly depend on ξ (see figure 7), and on the other hand the maximal field is not very large and still depends on ξ. However, with decreasing field, the vortex core volume substantially reduces which is disadvantageous for the data analysis as discussed above. Figure 19 shows a similar contour plot of $\chi^2(\lambda, \xi)$ for noisy data simulated using the NGL and ML models with parameters $\lambda_0 = 200$ nm, $\xi_0 = 4$ nm ($\kappa_0 = 50$), $\sigma_{g0} = 0.7$ mT, 20 million statistics, and $b_0 = 0.004$, 0.02, and 0.1. This corresponds approximately to the analysis of the simulated data that we discussed before. There is a substantial correlation between λ and ξ at all fields. For $b_0 = 0.1$ the analysis yields $\xi = 4(1)$ nm (correlated with λ), for $b_0 = 0.02$ only an upper limit of $\xi \simeq 5$ nm can be given, and for $b_0 = 0.004$ (0.082 T) the fit is practically independent of ξ at 20 million statistics. However, at unrealistically high statistics the dependence of χ^2 on λ and ξ becomes stronger (see figure 14), and the precision of the parameters extracted from the fit increases as the square root of the statistics. Another way of solving this problem was proposed by Riseman *et al* [17]: by simultaneously fitting several spectra measured at different fields with common values of the parameters λ and ξ. This has two advantages. (1) It effectively increases the statistics. (2) Since the correlation curve $\lambda(\xi)$ changes their slope with field (see figure 19), the total contour graph of $\chi^2(\lambda, \xi)$ will shrink, allowing a determination of the correct parameters. For example in the case of a high value of κ and extremely small field b, one can determine the correct value of λ (independently of the value of ξ), and with the known value of λ it is possible to evaluate a reliable value of ξ at high field by means of the correlation curve $\xi(\lambda)$. This procedure can be justified at least for conventional superconductors. Recently, Landau and Keller [32] reanalyzed μSR data for various conventional superconductors and convincingly demonstrated that in many cases type-II superconductors can be described by a field independent penetration depth. The present results are also relevant for the interpretation of small-angle neutron scattering (SANS) experiments in the mixed phase of type-II superconductors, since the strong correlation between λ and ξ is also present in Fourier components of the FLL [44].

We can conclude that in general a simultaneous determination of ξ and λ from μSR spectra without additional restrictions is not easy, regardless of the model used to describe the vortex state. At high κ and low fields there is practically no dependence of the spectra on ξ, and at high fields ξ is strongly correlated with λ. As demonstrated in figures 3, 5, and 7 this is independent of the value of κ and the model used. It is important to add that in our analysis of the μSR data using the advanced models, we used the same model for the simulations and the analysis, which reduces systematic errors to a minimum. In practice, there is often no adequate model for the description of the experimental μSR spectra, as for instance for unconventional superconductors such as the cuprate superconductors. In this case additional difficulties in the data analysis are expected. In the analysis of the

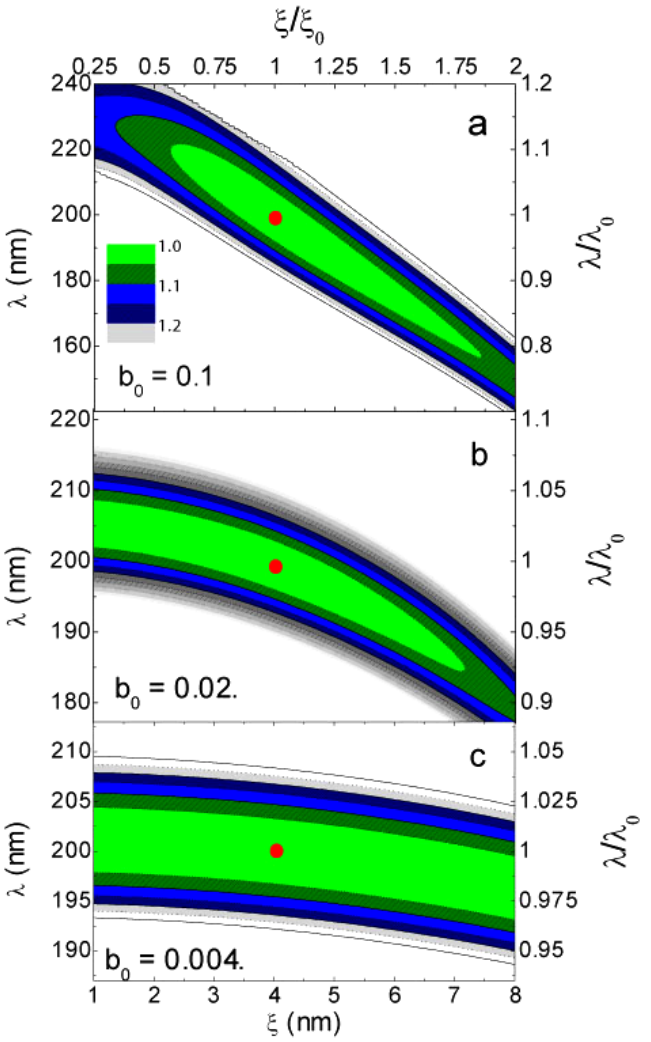

Figure 19. Contour plots of χ^2 as a function of λ and ξ for μSR spectra simulated using the parameters $\lambda_0 = 200$ nm, $\xi_0 = 4$ nm, $\sigma_{g0} = 0.7$ mT, 20 million counts, and $b_0 = 0.004$, 0.02, and 0.1. The results in (a) were obtained using the NGL model, and those in (b) and (c) were obtained using the ML model. There is a strong correlation of the fitted values of λ and ξ for high ($b_0 = 0.1$) and intermediate ($b_0 = 0.02$) fields, but nearly no correlation at low fields ($b_0 = 0.004$). The statistically scattered minimal value of χ^2 is normalized to 1. The real values of λ and ξ are indicated by the red point.

μSR spectra in section 5 we did not consider background signals arising from impurity fractions/phases in the sample and/or from muons stopping in the sample holder or other parts of the spectrometer. These background signals may be a hidden source of uncertainties in the determination of reliable parameters from μSR spectra. The introduction of additional fit parameters in the advanced models should be done only with great care, since already the existing minimal set of parameters of the models are, in general, difficult to extract.

6. Conclusions

We performed an analysis of the line shape of μSR spectra of type-II superconductors in the mixed state simulated using

four different models frequently adopted: (1) the modified London model (ML), (2) the London model with Gaussian cut-off (LG), (3) the analytical Ginzburg–Landau (AGL), and (4) the numerical Ginzburg–Landau (NGL) model. The dependence of the line shape on the penetration depth λ, the coherence length ξ, the applied magnetic field B, and the Gaussian smearing parameter σ_g is in agreement with previous studies [35, 38, 4]. It is discussed under what conditions these models can be used to describe the vortex state in extreme type-II superconductors. As a result, the ML model can be applied for fields $b = B/B_{c2} \leqslant 0.1$ (B_{c2} is the second critical field). On the other hand, the AGL and LG models can be applied over the whole range of fields, but in the range $b \simeq 10^{-2}-1$ they systematically deviate from the NGL model. It was shown that at low fields $b \leqslant 10^{-3}$ there is practically no dependence of the line shape on ξ. However, with increasing field, there is a strong dependence of the line shape on both λ and ξ, but the strong correlation between them makes it almost impossible to determine λ and ξ simultaneously. This is independent of $\kappa = \lambda/\xi$ and the model used. Additional restrictions for ξ (or λ) are needed to get rid of this correlation for reasonable statistics. Furthermore, it was shown that it is possible to determine λ and σ_g simultaneously, provided that ξ is fixed and the correlation between them is not too strong. In addition, it was demonstrated that the second-moment method (SM), frequently used for μSR data analysis, may yield reliable values for λ (within a few per cent) over whole field range $0 < b \lesssim 1$, provided that the vortex lattice disorder is not substantial. A multiple-Gaussian fit may give reliable values for the second moment and may approximate well the local magnetic field distribution in a type-II superconductor. In order to substantiate these conclusions made above, we performed virtual experiments by generating noisy μSR spectra with known parameters. The results of a comprehensive analysis of these μSR spectra are in full agreement with the conclusions drawn above.

Acknowledgments

We would like to acknowledge E H Brandt and I L Landau for valuable discussions. This work was partly supported by the Swiss National Science Foundation, the K Alex Müller Foundation, and the SCOPES GRANT No. IB7420-110784.

References

[1] Schenck A 1985 *Muon Spin Rotation Spectroscopy: Principles and Applications in Solid State Physics* (Bristol: Hilger)
[2] Dalmas De Réotier P and Yaouanc A 1997 *J. Phys.: Condens. Matter* **9** 9113
[3] Sonier J E, Brewer J H and Kiefl R F 2000 *Rev. Mod. Phys.* **72** 769
Sonier J E 2007 *Rep. Prog. Phys.* **70** 1717–55
[4] Brandt E H 2003 *Phys. Rev.* B **68** 054506
[5] Abrikosov A A 1950 *Zh. Eksp. Teor. Fiz.* **32** 1064
[6] Aeppli G, Cava R J, Ansaldo E J, Brewer J H, Kreitzman S R, Luke G M, Noakes D R and Kiefl R F 1978 *Phys. Rev.* B **35** 7129
[7] Harshman D R *et al* 1987 *Phys. Rev.* B **36** 2386
[8] Uemura Y J *et al* 1988 *Phys. Rev.* B **38** 909
[9] Pümpin B *et al* 1990 *Phys. Rev.* B **42** 8019
[10] Zimmermann P *et al* 1995 *Phys. Rev.* B **52** 541
[11] Aegerter C M and Lee S L 1997 *Appl. Magn. Reson.* **13** 75
[12] Lee S L 1999 *Muon Science* ed S L Lee, S H Kilcoyne and R Cywinski (Bristol: Institute of Physics Publishing) p 149
[13] Brandt E H 1988 *Phys. Rev.* B **37** 2349
[14] Yaouanc A, Dalmas de Réotier P and Brandt E H 1997 *Phys. Rev.* B **55** 11107
[15] Clem J R 1975 *J. Low Temp. Phys.* **18** 427
[16] Hao Z, Clem J R, McElfresh M W, Civale L, Malozemoff A P and Holtzberg F 1991 *Phys. Rev.* B **43** 2844
[17] Riseman T M *et al* 1995 *Phys. Rev.* B **52** 10569
[18] Yamashita A, Ishii K, Yokoo T, Akimitsu J, Hedo M, Inada Y, Onuki Y, Yamamoto E, Haga Y and Kadono R 1997 *Phys. Rev. Lett.* **79** 3771
[19] Miller R I, Kiefl R F, Brewer J H, Chakhalian J, Dunsiger S, Morris G D, Sonier J E and MacFarlane W A 2000 *Phys. Rev. Lett.* **85** 1540
[20] Ohishi K *et al* 2000 *Physica* B **289/290** 377
[21] Kadono R *et al* 2001 *Phys. Rev.* B **63** 224520
[22] Price A N, Miller R I, Kiefl R F, Chakhalian J A, Dunsiger S R, Morris G D, Sonier J E and Canfield P C 2002 *Phys. Rev.* B **65** 214520
[23] Ohishi K *et al* 2002 *Phys. Rev.* B **65** 140505(R)
[24] Miller R I, Kiefl R F, Brewer J H, Chakhalian J C, Dunsiger S, Price A N, Bonn D A, Hardy W H, Liang R and Sonier J E 2003 *Physica* B **326** 296
[25] Sonier J E, Callaghan F D, Miller R I, Boaknin E, Taillefer L, Kiefl R F, Brewer J H, Poon K F and Brewer J D 2004 *Phys. Rev. Lett.* **93** 017002
[26] Serventi S, Allodi G, De Renzi R, Guidi G, Romanó L, Manfrinetti P, Palenzona A, Niedermayer Ch, Amato A and Baines Ch 2004 *Phys. Rev. Lett.* **93** 217003
[27] Sonier J E 2004 *J. Phys.: Condens. Matter* **16** S4499
[28] Callaghan F D, Laulajainen M, Kaiser C V and Sonier J E 2005 *Phys. Rev. Lett.* **95** 197001
[29] Laulajainen M, Callaghan F D, Kaiser C V and Sonier J E 2006 *Phys. Rev.* B **74** 054511
[30] Salman Z *et al* 2007 *Phys. Rev. Lett.* **98** 167001
[31] Sonier J E *et al* 2007 *Phys. Rev.* B **76** 134518
[32] Landau I L and Keller H 2007 *Physica* C **466** 131
[33] Weber M *et al* 1993 *Phys. Rev.* B **48** 13022
[34] Khasanov R, Shengelaya A, Maisuradze A, La Mattina F, Bussmann-Holder A, Keller H and Müller K A 2007 *Phys. Rev. Lett.* **98** 057007
[35] Brandt E H 1977 *J. Low Temp. Phys.* **26** 709
Brandt E H 1988 *J. Low Temp. Phys.* **73** 355
[36] Brandt E H 1997 *Phys. Rev. Lett.* **78** 2208
[37] Delrieu J M 1972 *J. Low Temp. Phys.* **6** 197
[38] Sidorenko A D, Smilga V P and Fesenko V I 1990 *Hyperfine Interact.* **63** 49
[39] Dalmas de Réotier P, Gubbens P C M and Yaouanc A 2004 *J. Phys.: Condens. Matter* **16** S4687
[40] Tinkham M 1996 *Introduction to Superconductivity* 2nd edn (New York: McGraw-Hill)
Pümpin B *et al* 1990 *J. Less-Common Met.* **164/65** 994
[41] Maisuradze A *et al* 2008 unpublished
[42] Khasanov R, Landau I L, Baines C, La Mattina F, Maisuradze A, Togano K and Keller H 2006 *Phys. Rev.* B **73** 214528
[43] Rainer D and Usadel K D 1974 *Phys. Rev.* B **9** 2409
[44] Chang J, Mesot J, Gilardi R, Kohlbrecher J, Drew A J, Divakar U, Lister S J, Lee S L, Brown S P, Charalambous D, Forgan E M, Dewhurst C D, Cubitt R, Momono N and Oda M 2006 *Physica* B **385/386** 35